

Immobilization of Hg(II) by Coprecipitation in Sulfate-Cement Systems

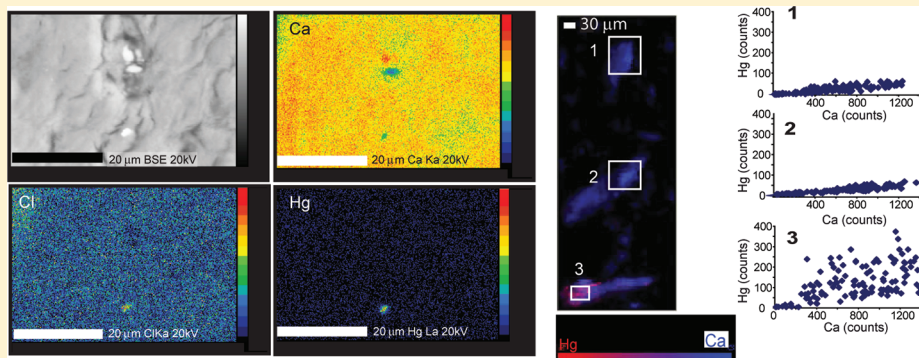
Susana Serrano,^{†,‡,*} Dimitri Vlassopoulos,[‡] Brad Bessinger,[§] and Peggy A. O'Day[†]

[†]School of Natural Sciences, University of California, Merced, California 95343, United States

[‡]Anchor QEA, LLC, Portland, Oregon 97204, United States

[§]S. S. Papadopoulos & Associates Inc., Portland, Oregon 97204, United States

Supporting Information



ABSTRACT: Uptake and molecular speciation of dissolved Hg during formation of Al- or Fe-ettringite-type and high-pH phases were investigated in coprecipitation and sorption experiments of sulfate-cement treatments used for soil and sediment remediation. Ettringite and minor gypsum were identified by XRD as primary phases in Al systems, whereas gypsum and ferrihydrite were the main products in Hg–Fe precipitates. Characterization of Hg–Al solids by bulk Hg EXAFS, electron microprobe, and microfocused-XRF mapping indicated coordination of Hg by Cl ligands, multiple Hg and Cl backscattering atoms, and concentration of Hg as small particles. Thermodynamic predictions agreed with experimental observations for bulk phases, but Hg speciation indicated lack of equilibration with the final solution. Results suggest physical encapsulation of Hg as a polynuclear chloromercury(II) salt in ettringite as the primary immobilization mechanism. In Hg–Fe solids, structural characterization indicated Hg coordination by O atoms only and Fe backscattering atoms that is consistent with inner-sphere complexation of $\text{Hg}(\text{OH})_2^0$ coprecipitated with ferrihydrite. Precipitation of ferrihydrite removed Hg from solution, but the resulting solid was sufficiently hydrated to allow equilibration of sorbed Hg species with the aqueous solution. Electron microprobe XRF characterization of sorption samples with low Hg concentration reacted with cement and FeSO_4 amendment indicated correlation of Hg and Fe, supporting the interpretation of Hg removal by precipitation of an Fe(III) oxide phase.

1. INTRODUCTION

Mercury (Hg), derived from both natural and anthropogenic sources, is one of the most toxic elements present in soils and sediments. Bacterial methylation of inorganic Hg is the primary pathway for generation of methylmercury species, which bioaccumulate and biomagnify in the food chain.¹ Fish consumption is the main source of human exposure to Hg as methylmercury.² Because Hg methylation depends on bacterial bioavailability of inorganic Hg,³ an effective remediation strategy is to isolate and stabilize Hg in nonbioaccessible media to minimize the potential for methylation. Cementitious amendments, such as Portland-type and related cements, are attractive for soil and sediment stabilization because of their ability to immobilize and isolate a variety of inorganic contaminants, and their recalcitrance under different environmental conditions.⁴ In sulfate-type Portland cements, ettringite is one of the main mineral products resulting from cement

hydration. Because of its ability to bind both cation and anion contaminants through substitution of Ca^{2+} , Al^{3+} , SO_4^{2-} or OH^- , or through sorption on surfaces, ettringite has been the subject of numerous studies.^{5–11}

Mercury stabilization using sulfate-cement amendments may be particularly useful in alkaline chemical systems such as the stabilization of fly ash wastes or sediment remediation associated with contamination from Hg-cell chlor-alkali manufacturing facilities. Another application is the addition of cement-type amendments to stabilize Hg in contaminated sediments dredged from waterways before either disposal or reuse.^{12,13} Solidification and stabilization of Hg using

Received: August 22, 2011

Revised: April 23, 2012

Accepted: May 17, 2012

Published: May 17, 2012

cementitious materials has been studied previously, but most studies examined amendment effectiveness by leaching tests, with little direct evidence of possible mechanisms responsible for Hg retention.^{14–20} Proposed Hg retention mechanisms in cement included precipitation of HgO(s) ,¹⁶ or physical encapsulation after cement treatment.^{14,18} None of these prior studies used spectroscopic methods to examine molecular-scale Hg speciation in amendment reaction products to help deduce sequestration mechanisms.

Mercury speciation and coordination chemistry in solution at equilibrium conditions have been well documented. Hydrolysis reactions determine Hg(II) aqueous speciation in the absence of complexing ligands. At low pH in the absence of Cl^- , Hg forms a hexaqua ion $[\text{Hg}(\text{H}_2\text{O})_6]^{2+}(\text{aq})$ ²¹ and as pH increases, the dominant species is $\text{Hg}(\text{OH})_2(\text{aq})$. In these aqueous complexes, two of the Hg–O bonds are shortened while two bonds are lengthened, giving the appearance of two-coordinated Hg complex.²¹ At dissolved Cl^- concentrations typical of natural environments, Hg forms a $\text{HgCl}_2(\text{aq})$ complex with a similar linear geometry between Hg and Cl. At high Cl^- concentrations, HgCl_3^- and tetrahedral HgCl_4^{2-} are the major species.²² Strong complexing ligands such as Cl^- influence Hg speciation by formation of aqueous complexes that change Hg affinity for mineral surfaces. Prior studies have shown that, in the presence of dissolved Cl^- , Hg adsorption on goethite is shifted to higher pH^{23,24} and that Hg uptake is reduced on goethite, alumina, and bayerite.^{25,26}

In this study, formation of Al- or Fe-etrtringite and related solid products at high pH in the presence of dissolved Hg(II) was examined using spectroscopic and microscopic spatial analysis methods to identify microscale mechanisms of Hg incorporation by cementitious product phases. These coprecipitation experiments were compared with Hg(II) sorption by Portland cement and iron sulfate mixtures at lower total Hg concentration. The model experimental systems investigated here lend insight into the importance of both equilibrium and kinetic factors in controlling the formation of reaction products in high-pH cement-type systems used for remediation.

2. MATERIALS AND METHODS

2.1. Mercury Coprecipitation and Sorption Experiments and Extractions. Coprecipitation experiments with and without dissolved Hg were performed following the method for synthesis of ettringite described by Odler and Abdulmaula²⁷ and Warren and Reardon,⁶ with some modifications. For the Al-coprecipitate (Al-cpt), 10 mL of 0.229 M CaO(aq) were added to 10 mL of 0.038 M $\text{Al}_2(\text{SO}_4)_3(\text{aq})$ and adjusted to pH 12.5 using 10 mL of 1.0 M NaOH. The Hg-containing analog (Hg-Al-cpt) was prepared identically with the addition of 10 mL of 0.35 mM $\text{HgCl}_2(\text{aq})$ in synthetic seawater²⁸ to the 1.0 M NaOH solution ($\text{Hg}_{\text{tot}} = 0.25 \text{ mM}$). An Fe coprecipitate (Fe-cpt) was synthesized by mixing 10 mL 0.229 M CaO(aq) and 10 mL 0.039 M $\text{Fe}_2(\text{SO}_4)_3 \cdot 5\text{H}_2\text{O}$, and adjusting pH to 12.5 using 1.0 M NaOH. A Hg precipitate (Hg-Fe-cpt) was prepared identically with the addition of 10 mL of 0.35 mM $\text{HgCl}_2(\text{aq})$ dissolved in synthetic seawater. Reactants were mixed in Nalgene Oak Ridge high speed PPCO tubes in a N_2 -filled glovebox to exclude $\text{CO}_2(\text{g})$ and all solutions were degassed with N_2 before mixing. Suspensions were shaken at room temperature for 48 h, measured for pH, and centrifuged (10 000 rpm for 10 min). Supernatant solutions were filtered through 0.45 μm filters under N_2 -gas atmosphere. All solutions

were kept under acidic conditions until analysis using ICP-MS for Hg and ICP-OES for major elements (Ca, S, Al, and Fe) (see Supporting Information (SI) for details). After removal of supernatant solutions, solid phases were washed two times with deionized water, dried under N_2 , and split for analyses. The exchangeable Hg fraction in the coprecipitate samples (Hg-Al-cpt and Hg-Fe-cpt) was extracted using 5 mL of 1.0 M $\text{MgCl}_2(\text{aq})$ by shaking at room temperature for 1 h.²⁹ Total Hg concentration was determined by microwave digestion in aqua regia (HCl:HNO_3 3:1) and analysis by ICP-MS.

Mercury sorption experiments at lower total Hg concentration ($\text{Hg}_{\text{tot}} = 0.01 \text{ mM}$) were performed by mixing cement amendments (Portland cement + FeSO_4) with 0.01 mM HgCl_2 . Following equilibration for 1, 7, or 30 days, sequential chemical extractions were carried out to determine the Hg exchangeable fraction (0.1 M $\text{MgCl}_2(\text{aq})$) and Hg associated with poorly crystalline phases (0.2 M acidic ammonium oxalate solution (AAO)). Experimental details are described in the SI.

For XAS reference spectra, $\text{HgCl}_2(\text{s})$ was used as obtained from Fisher Scientific. A solution of $\text{HgCl}_2(\text{aq})$ (100 ppm Hg) was prepared from the $\text{HgCl}_2(\text{s})$ salt in deionized water (pH 4.5). HgO(s) (montroydite) was precipitated in the laboratory by the addition of excess NaOH solution to an aqueous solution containing 50 g $\text{HgCl}_2(\text{s})$. The solid was filtered and washed to remove excess chloride. $\text{Hg}_3(\text{SO}_4)\text{O}_2(\text{s})$ (schuetteite) was precipitated after the addition of 150 mL of 0.093 mM $\text{Hg}(\text{NO}_3)_2 \cdot \text{H}_2\text{O(aq)}$ into 0.3 M $\text{Fe}_2(\text{SO}_4)_3$ solution at pH 1.7 at 98 °C. Mercury sorbed on goethite (Hg/goethite) was prepared by reacting 50 mL of 0.5 mM $\text{Hg}(\text{NO}_3)_2$ solution with 0.5 g of poorly crystalline goethite synthesized according to the method of Schwertmann and Cornell³⁰ for 24 h (approximate Hg surface coverage of 0.6 $\mu\text{mol Hg/m}^2$). Following equilibration, the sample was centrifuged at 10 000 rpm for 15 min and the supernatant solution removed. Solid reference materials were stored wet. The identity of all solids was confirmed by X-ray diffraction (XRD).

2.2. X-ray Diffraction (XRD). X-ray diffraction analysis was performed on beamline 11–3 at the Stanford Synchrotron Radiation Lightsource (SSRL) using a Si(111) monochromator with a spot size of $0.15 \times 0.15 \text{ mm}$ between 3° and $124^\circ 2\theta$ in 0.006° steps. Samples were dispersed on adhesive tape and sealed with a second piece of tape. The XRD patterns were calibrated with a LaB_6 standard and converted to wavelength using nonlinear curve fit and Bragg fit equations. Mineral identification was performed using the ICDD reference database with the Jade software package (MDI Products).

2.3. Electron Microprobe and Microfocused-XRF. Chemical mapping using electron microprobe X-ray fluorescence (XRF) was performed on solid samples embedded in epoxy and made into petrographic thin sections. Mapping was done with a CAMECA SX100 Ultra electron microprobe (Department of Planetary Sciences, University of Arizona) operating at 20 keV and 20 nA, and equipped with wavelength dispersive spectrometry (WDS) detectors. Maps were collected with a step size of 0.2 μm and a dwell time of 8 ms.

Synchrotron microfocus μ -XRF data were collected at the SSRL on beamline 2–3 using a single element Si Vortex (SSI) with Si(220) double crystal monochromator. Solid samples were finely ground and dusted as a thin layer on adhesive tape. X-ray energy was tuned to 12,300 eV and maps were collected in continuous raster scanning mode for Hg, Ca, Fe, S, and Al in solid samples. Fluorescence maps were analyzed using the Microanalysis Toolkit³¹ and element count rates were

normalized to the measured intensity of the incident X-ray beam (I_0).

2.4. X-ray Absorption Spectroscopy (XAS). Sulfur K-edge X-ray absorption spectra were collected on beamline 4–3 at the SSRL operating at 3.0 GeV and 100–200 mA. Methods are described in the SI. Spectral analysis was performed with the program SIXPAK.³¹ Background before the edge was subtracted using a linear fit to the pre-edge region and spectra were normalized to the postedge step height. Mercury L_{III}-edge X-ray absorption spectra were collected on either beamline 4–1 or 11–2 at the SSRL operating at 100–200 mA. Analyses of the Hg EXAFS spectra were performed with the program EXAFSPAK.³² Details of data collection and analysis are described in SI.

2.5. Equilibrium Calculations. Thermodynamic calculations for coprecipitate experiments were performed using the Geochemist's Workbench modeling package with a modified version of the Lawrence Livermore National Laboratory (LLNL) thermodynamic database³³ augmented with the "cemdata 07" thermodynamic database³⁴ (Table S4 in SI) and with recently compiled thermodynamic values for inorganic Hg species.³⁵

3. RESULTS

3.1. Chemical Composition of Reaction Products. Analysis of the digested product phases indicated that 3.90 mmol/kg (94% of the total Hg added (Hg_{tot}))) and 2.64 mmol/kg (90% Hg_{tot}) were retained in the Hg-Al-cpt and Hg-Fe-cpt solids, respectively, after 2 days of reaction (Table S1 in SI). The fraction of exchangeable Hg was 0.59 mmol/kg (20% Hg_{tot}) and 1.04 mmol/kg (25% Hg_{tot}) for the Hg-Al-cpt and Hg-Fe-cpt solids, respectively. The molar ratio of total Ca to S in Hg-Fe-cpt solids was close to 1:1 (~300 mmol/kg), whereas Ca was greater than S, and significantly higher (4613 and 2551 mmol/kg, respectively) in Hg-Al-cpt solids (Table S1 in SI). Measured pH after 2 days of reaction in Hg-Fe-cpt and Hg-Al-cpt experiments was 12.6 and 12.4, respectively.

Sorption experiments with cement and FeSO₄ amendment showed that between 91% and 99% of the total Hg added to the system (=0.01 mM) was retained in the solid phases after 1, 7, and 30 days of reaction (Table S3 in SI). Mercury uptake increased with reaction time, and Hg was associated primarily with the residual fraction, with less than 1% of the total Hg adsorbed associated with the exchangeable and acid oxalic-extracted fractions.

3.2. X-ray Diffraction. Bulk XRD analysis of coprecipitate products indicated that ettringite was the primary mineral phase in both Al-cpt and Hg-Al-cpt products; gypsum and bayerite were also identified in the latter system (SI Figure S1). In the Hg-Fe-cpt products, gypsum was the primary mineral phase and ettringite was present as a minor phase (SI Figure S1). No crystalline Fe(III) oxide minerals were identified by XRD in either the coprecipitate or sorption samples, but the formation of an amorphous Fe-oxide phase such as ferrihydrite is likely based the observation, in both coprecipitate and sorption samples, of an orange precipitate similar to that noted in prior studies.⁷ In the Fe-cpt system without Hg, gypsum was absent and a Ca-Fe-sulfate-hydrate phase and calcite (as a minor phase) were identified. However, the stoichiometry of the Ca-Fe-sulfate-hydrate phase that best matched the reflections in the diffractogram is uncertain (reference pattern 00–044–0601 in the ICDD database) and several reflections could not be identified. The presence of less crystalline, unidentified mineral

phases in the XRD pattern was indicated by broad peaks, but none could be attributed to ferrihydrite.³⁶

3.3. Sulfur XAS. Normalized S XANES of coprecipitate samples were compared with reference spectra of CaSO₄·2H₂O(s) (gypsum) and HgSO₄(s) (Figure 1). Spectra of Al-

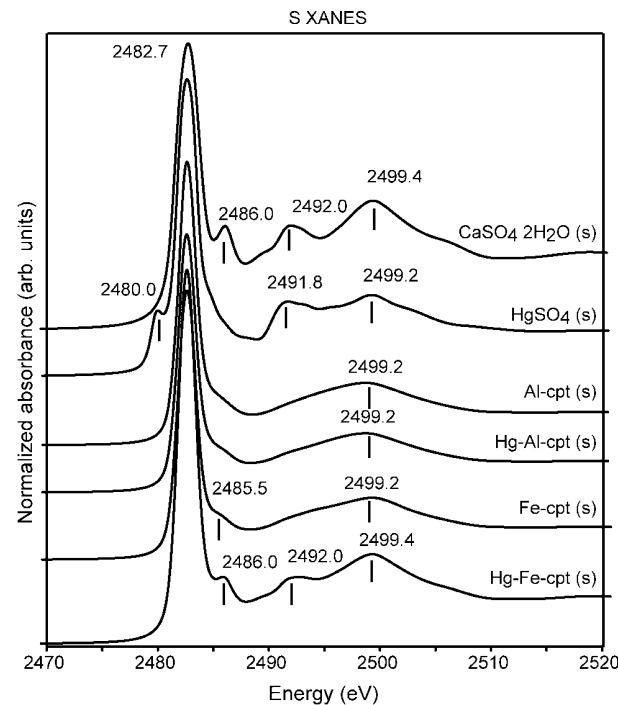


Figure 1. Normalized sulfur K-edge XANES spectra of Hg-Al-cpt and Hg-Fe-cpt solid phases compared to precipitates without Hg (Al-cpt, Fe-cpt) and to sulfate reference compounds (gypsum, CaSO₄·2H₂O, and HgSO₄).

cpt and Hg-Al-cpt showed similar XANES features that were characterized by an absorption maximum at 2482.7 eV and a postedge absorption feature at 2499.2 eV. These results indicate similar bulk S coordination in both solid products, consistent with ettringite (identified by XRD) as the major mineral phase. The S XANES spectrum of Fe-cpt was slightly different. It showed a small feature at 2485.5 eV in addition to the feature at 2499.2 eV observed in Al-cpt and Hg-Al-cpt spectra. These differences are likely related to the presence of a Ca-Fe-sulfate-hydrate phase rather than ettringite as the main crystalline phase from XRD analysis (SI Figure S1). The spectrum of Hg-Fe-cpt is characterized by three main postedge absorption features at 2486.0, 2492.0, and 2499.4 eV, which correspond to features observed in gypsum and are consistent with the XRD identification of gypsum as the main crystalline phase (Figure S1).

3.4. Mercury XAS. Analyses of crystalline Hg reference compounds (described in SI) were used to constrain unknown parameters (σ^2 , S_0^2) and to provide a basis for the identification of backscattering shells in unknown spectra. Mercury X-ray absorption spectra of coprecipitate samples (Hg-Al-cpt, Hg-Fe-cpt) are compared in Figure 2 with spectra of Hg dissolved in aqueous solution (HgCl₂(aq)) and to Hg sorbed to goethite (Hg/goethite). Although these samples were prepared under different experimental conditions (pH, initial Hg salt, presence or absence of Cl[−]), similar features were observed in the Hg XANES, particularly among the Fe-free compared to Fe-present systems (Figure 2a,b). For all spectra, similarities in the main

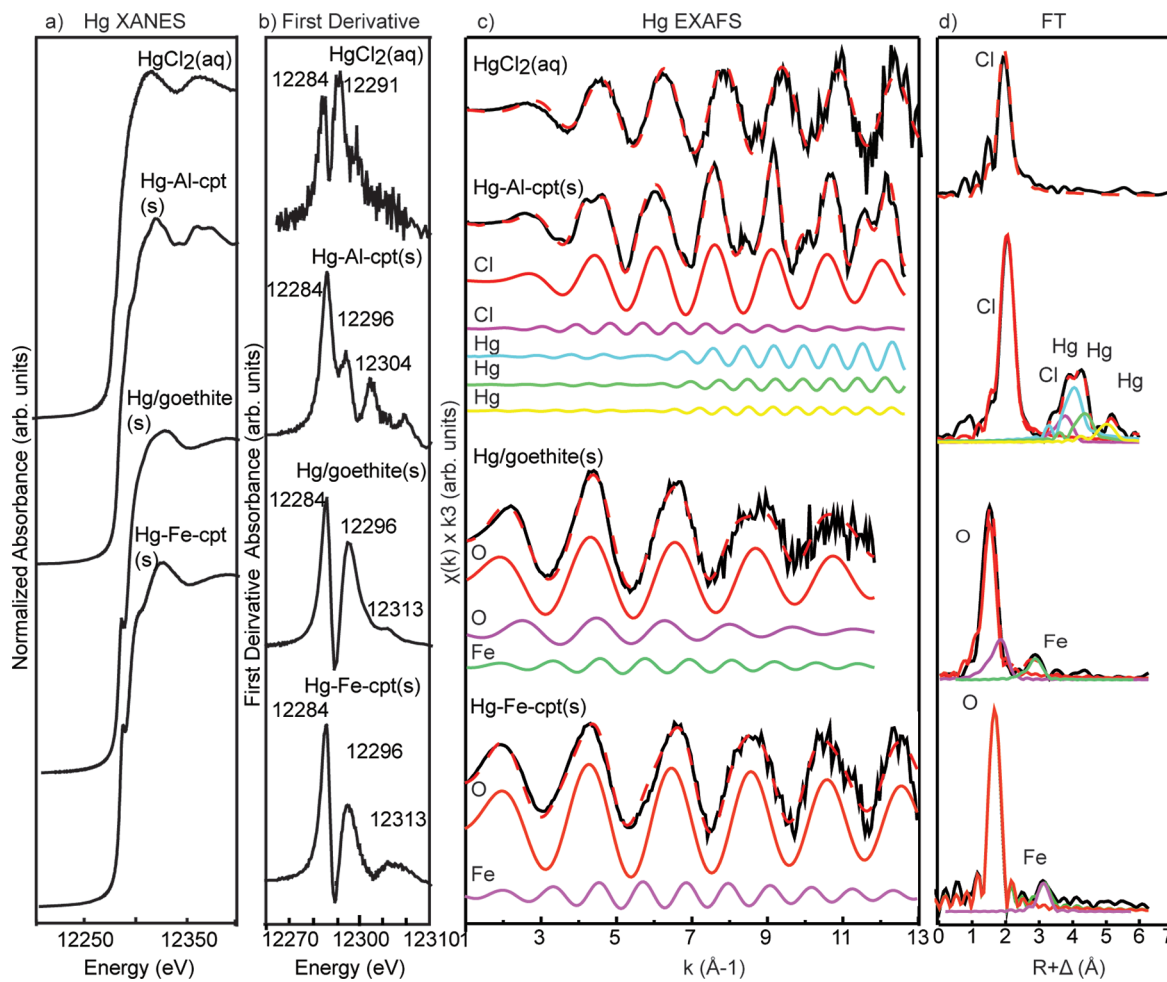


Figure 2. Mercury L(III)-edge XANES and corresponding first-derivative spectra, and EXAFS and Fourier transforms (FT) of the solid phases Hg-Al-cpt, Hg-Fe-cpt, and Hg(II) adsorbed on goethite (Hg/Goethite), and a 0.5 mM solution of $\text{HgCl}_2(\text{aq})$. Deconvolution of single-scattering paths are shown in the EXAFS and FT of Hg-Al-cpt and Hg-Fe-cpt. Solid lines are data and dashed lines are nonlinear least-squares fits (numerical fit results are shown in Table 1).

features and inflections (observed in the first-derivative spectra) were found. Comparison of the XANES spectra of Hg-Al-cpt and Hg in solution showed that $\text{HgCl}_2(\text{aq})$ had two main inflections at 12 284 eV and 12 291 eV, but in the same energy range, Hg-Al-cpt was characterized by three inflections at 12 284, 12 296, and 12 304 eV. The energy positions and amplitudes of inflections in the Hg-Fe-cpt XANES spectrum were similar to those of Hg/goethite, and differed slightly from the Fe-free spectra. In particular, the amplitude of the inflection at 12 296 eV was more prominent, and the inflection at 12 304 eV was low or absent, in Hg-Fe-cpt and Hg/goethite spectra compared to Hg-Al-cpt.

Quantitative EXAFS analysis of the HgCl_2 solution was based on the assumption that the predominant aqueous species was $\text{HgCl}_2(\text{aq})$, as indicated by thermodynamic calculations. Fit results showed Hg coordination by two Cl atoms (N fixed) at a distance of 2.45 Å. In the EXAFS analysis of Hg-Al-cpt, a first-shell of ~3 Cl atoms at a distance of 2.51 Å was identified (Table 1), which is longer than the Hg-Cl distance (2.28 Å) derived from fitting of the $\text{HgCl}_2(\text{s})$ standard reference (SI Table S5) but similar to the aqueous complex. The first coordination shell could not be fit with any O atoms, and S (associated with sulfate groups) could not be fit in the spectrum at any distance. Trial-and-error tests based on prior studies of

Table 1. Results of Hg EXAFS Fits^a

sample	A-B	N	$R (\text{\AA})$	$\sigma^2 (\text{\AA}^2)$	$\Delta E_0 (\text{\AA})$	χ^2
$\text{HgCl}_2(\text{aq})$ (0.5 mM solution)	Hg-Cl	2.0 ^b	2.45	0.0023	-3.15	0.40
Hg-Al-cpt(s)	Hg-Cl	3.0	2.51	0.0043 ^b	-4.65	0.19
	Hg-Hg	3.0	4.14	0.0050 ^b		
	Hg-Cl	4.2	4.24	0.010 ^b		
	Hg-Hg	2.0	4.46	0.0043 ^b		
	Hg-Hg	4.0	5.16	0.0087 ^b		
Hg/goethite(s)	Hg-O	1.2	2.00	0.003 ^b	-4.90	0.07
	Hg-O	2.0	2.45	0.015 ^b		
	Hg-Fe	0.7	3.46	0.006 ^b		
Hg-Fe-cpt(s)	Hg-O	1.7	2.03	0.003 ^b	-0.84	0.06
	Hg-Fe	1.0	3.49	0.006 ^b		

^aA-B is the absorber-backscatterer pair; N is the number of backscattering atoms at distance (R); σ^2 (Debye-Waller term) is the absorber-backscatterer mean-square relative displacement; ΔE_0 is the energy shift in the least-squares fit; χ^2 is a reduced least-squares goodness-of-fit parameter (=F-factor)/(no. of points - no. of variables); scale factor (S^2_0) fixed at 0.9. ^bParameter fixed in least-squares fit. ^cHg(II) sorbed to synthetic goethite.

the structure of poly mercury-chloride complexes and solids were done to determine the local structure around Hg in the

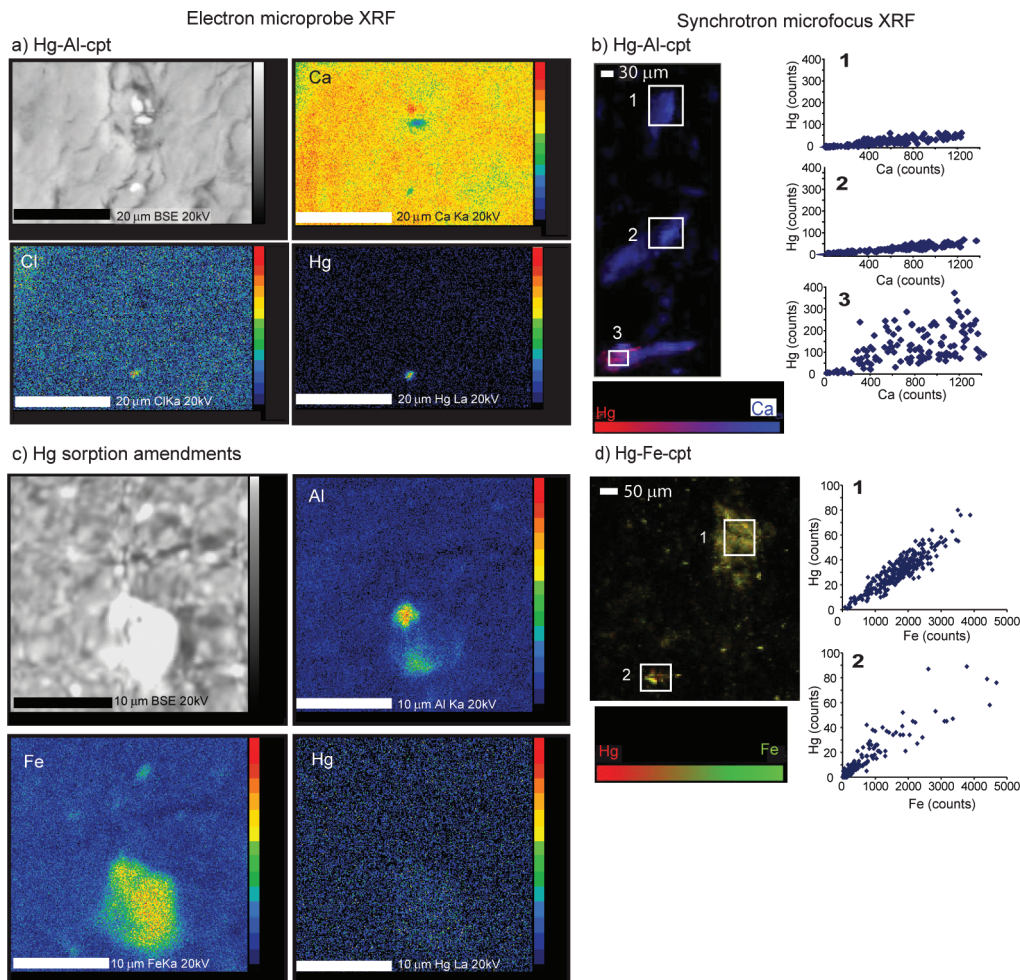


Figure 3. (a) Backscattered electron (BSE) image and element fluorescence maps from electron microprobe (petrographic thin section) of Hg-Al-cpt; (b) synchrotron microfocused X-ray fluorescence (μ -XRF) element maps and Hg–Ca correlation plots from the areas indicated (powdered sample) of Hg-Al-cpt; (c) BSE image and element fluorescence maps from electron microprobe of Hg sorbed to cement and FeSO_4 amendment (aged for 12 months); (d) synchrotron μ -XRF element maps and Hg–Fe correlation plots from the areas indicated of Hg-Fe-cpt.

Hg-Al-cpt. In the final fit, four neighboring atomic shells of Hg and Cl beyond the first Cl shell were determined (Table 1). Based on the analyses of Hg reference compounds (Figure S2, S3, and Table S5 in SI), Hg dominates the EXAFS as a strong backscattering atom compared to lighter elements that may be present in the spectrum.

In contrast to the Fe-free systems, Hg coordination by Cl was not found in coprecipitate samples with Fe present (Hg concentrations in sorption samples were too low for XAS). Overall, Cl^- (0.01 M) and SO_4^{2-} (0.1 M) in solution in the Hg–Fe-cpt system did not produce any large structural change in the average Hg coordination compared to the chloride and sulfate-free Hg/goethite sample, but minor differences in the EXAFS spectra were observed. Fits of the Hg/goethite(s) spectrum indicated two O shells at 2.00 and 2.45 Å and one Fe shell at 3.46 Å (Table 1). Results for Hg-Fe-cpt showed only one O shell at 2.03 Å and one Fe shell at 3.49 Å. The Hg–O distances at 2.00 and 2.03 Å in Hg/goethite(s) and Hg-Fe-cpt, respectively, are similar to the Hg–O distances in the solid reference compounds $\text{HgO}(s)$, and $\text{Hg}_3(\text{SO}_4)\text{O}_2$ (2.03 and 2.06 Å, respectively, SI Table S3), and also to Hg coordination in the aqueous species $\text{Hg}(\text{OH})_2^{0,21,37}$. The EXAFS results are consistent with typical 2 + 4 geometry of Hg, with two short Hg–O ligands that give the appearance of Hg coordinated

linearly by O atoms, and four long Hg–O bonds completing the octahedral Hg coordination. The presence of a second O shell in Hg/goethite(s) at 2.45 Å is shorter than similar distances observed in crystalline compounds such as montroydite (with Hg–O fitted distance of 2.82 Å) or schuetteite (with Hg–O fitted distance of 2.53 Å), but similar to the average Hg–O distance of 2.42 Å for octahedrally coordinated $\text{Hg}(\text{H}_2\text{O})_6^{2+}(\text{aq})$.³⁷ The low amplitude of the 2.45 Å O shell in the Hg/goethite spectrum, and its absence in the Hg-Fe-cpt spectrum, indicate structural disorder in the Hg coordination shell. However, backscattering amplitude from second-neighbor Fe atoms was stronger in the Hg-Fe-cpt spectrum than in the Hg/goethite spectrum (Figure 2).

3.5. Electron Microprobe and μ -XRF. Element fluorescence maps from electron microprobe and synchrotron μ -XRF spectroscopy of Hg-Al-cpt are shown in Figure 3. Microprobe results using both electron backscattering and element fluorescence mapping indicated a region on the order of 1 μm in diameter with highly concentrated Hg in a mapping area of 45 $\mu\text{m} \times 30 \mu\text{m}$ (Figure 3a). Fluorescence mapping indicated correlation of Hg with Cl, but a lower Ca concentration relative to the surrounding particle, in the high-Hg region. Larger areas of elevated Hg ($\sim 30 \mu\text{m}$) were identified by synchrotron μ -XRF maps of the same Hg-Al-cpt

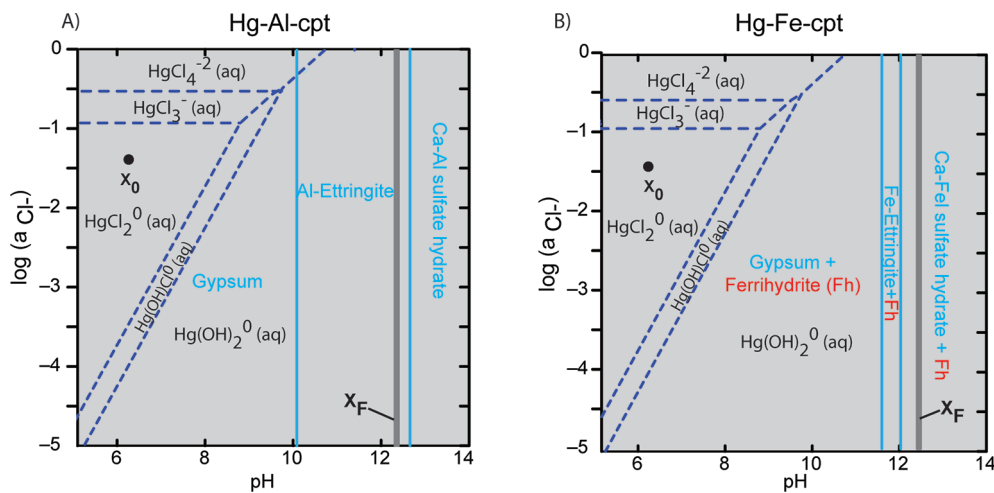


Figure 4. Equilibrium phase relations and solution speciation as a function of log activity of Cl^- ($\log (a_{\text{Cl}^-})$) and pH calculated using the initial composition of Hg-Al-cpt (a) and Hg-Fe-cpt (b) systems. Diagrams show dissolved Hg species (dark blue dashed lines), solid Ca phases (shaded, solid light blue lines), and solid Fe phases (named in red). X_0 (solid point) represents initial Cl^- and pH, and X_F (shaded line) represent final pH of solutions. Ca-Al-sulfate hydrate: $\text{Ca}_4\text{Al}_2(\text{SO}_4)(\text{OH})_{12} \cdot 6\text{H}_2\text{O}$ and Ca-Fe-sulfate hydrate: $\text{Ca}_4\text{Fe}_2(\text{SO}_4)(\text{OH})_{12} \cdot 6\text{H}_2\text{O}$.

sample (Cl was not mapped) (Figure 3b). Regions of elevated Hg indicated a weak correlation with Ca in some areas, similar to electron microprobe results, and an absence of Hg in other high-Ca areas. Electron microprobe maps of sorption samples with low Hg concentration reacted with cement and FeSO_4 amendment showed a correlation between regions of high Fe (on the order of 5–10 μm in diameter) and areas of Hg elevated just above background (Figure 3c). Element μ -XRF maps of Hg-Fe-cpt samples with higher total Hg showed diffuse areas of high Fe (~ 10 –50 μm) correlated with Hg fluorescence above background counts (Figure 3d). Differences in the size of high Hg-regions between electron microprobe and μ -XRF maps can be attributed partly to sample preparation. For electron microprobe, samples were embedded in epoxy and made into a petrographic thin section, but for μ -XRF maps, powdered samples were dispersed on tape, and particles may have been aggregated.

4. DISCUSSION

4.1. Mercury Speciation from EXAFS and Spatial Analysis. Based on Hg XAS and microprobe results, distinctly different modes of Hg uptake were observed in Hg-ettringite coprecipitation with Al or Fe. In the Al-Hg coprecipitate, EXAFS and microprobe analyses suggest that Hg is likely concentrated as a polynuclear or nanoparticulate chloromercury(II) anionic species such as $[\text{Hg}_x\text{Cl}_y]^{n-}$ in a chloromercury salt-type phase. Chloromercury salts exhibit a wide structural diversity and variable composition.³⁸ Although most structural characterization has been performed on organo-Hg salts,²² $\text{Hg}_x\text{Cl}_y^{n-}$ stoichiometries were identified in inorganic salts, such as the “double salt” $[\text{CaCl}_2]_2[\text{HgCl}_2]_{11} \cdot 16\text{H}_2\text{O}$ containing $[\text{Hg}_6\text{Cl}_{13}]^-[Hg_5\text{Cl}_{13}]^{3-}$ clusters,³⁹ or the MgHg_3Cl_8 salt.⁴⁰ A range of Hg-Cl distances have been reported, depending on whether Cl is bridging between Hg atoms, with longer distances in general when Cl acts as a bridge.⁴¹ Structural results from EXAFS for Hg-Al-cpt gave an average Hg-Cl distance of 2.51 Å for ~3 Cl atoms in the first coordination shell. The Hg-Cl first-shell distance from the EXAFS fit is in the range of Hg-Cl distances observed for tetrahedral coordination in HgCl_4 ,⁴¹ which may suggest a distorted tetrahedral geometry. In addition, the presence of

multiple Hg atoms at longer distances (4.14, 4.46, and 5.16 Å) is consistent with the precipitation of a Hg-chloride-salt particle that is presumably balanced by Ca^{2+} atoms not detected in the EXAFS spectrum. Electron microprobe and synchrotron μ -XRF imaging indicated that Hg was rare and not uniformly distributed in the Hg-Al-cpt, but rather was concentrated in small particles, possibly as inclusions in high-Ca minerals.

In the Hg-Fe coprecipitate, Hg EXAFS analyses indicated that Hg coordinates only with O and Fe ligands in the first and second coordination shells, respectively, at slightly longer distances compared with the Hg/goethite EXAFS spectrum, which was also fit with a second low-amplitude Hg-O shell. Differences in local Hg coordination between these samples may result from the different pH (pH 6.5 for Hg/goethite and 12.6 for Hg-Fe-cpt) and different sample preparation (sorption versus coprecipitation) used for each. Second-neighbor Hg-Fe distances in both samples (3.46 and 3.49 Å) were slightly longer than the Hg-Fe distance (3.40 Å) reported previously for Hg sorption on goethite in one study.⁴² These Hg-Fe distances are significantly longer than the Hg-Fe distances (3.19–3.29 Å) reported in other studies for Hg complexes on goethite surfaces.^{25,26,43} These prior studies have attributed the observed differences in Hg-Fe distances to the presence of monodentate (longer distance) and bidentate (shorter distance) inner-sphere sorption complexes on goethite. In the Hg-Fe-cpt sample, stronger backscattering from second-neighbor Fe atoms is consistent with coprecipitation of Hg with ferrihydrite from solution, with higher surface area and more sorption sites, compared to sorption of Hg on an existing Fe(III) oxide surface for Hg/goethite. No evidence was found for the formation of ternary Hg-Cl species,^{5,24,25,43} or for ternary Hg-SO₄ species.²⁵ In both low concentration sorption samples and high concentration coprecipitates, elemental fluorescence mapping indicated a correlation of high Fe areas with weakly elevated Hg concentrations in diffuse particles, supporting the interpretation of Hg removal by precipitation of an Fe(III) oxide phase.

4.2. Equilibrium Analysis and System Kinetic Limitations. Ettringite was identified by XRD as the primary mineral phase in the Hg-Al-cpt (with minor gypsum) and Al-cpt systems, whereas gypsum and a Ca-Fe-sulfate-hydrate

phase were the primary crystalline phases in the Hg–Fe-cpt and Fe-cpt systems, respectively. These results were corroborated by qualitative comparisons of S-XANES spectra of the experimental systems with reference compound spectra, and in agreement with bulk chemistry of the solids. Thermodynamic phase relations at the experimental conditions of this study as a function of Cl^- activity and pH indicate that Al-ettringite is stable at pH between ~10 and 12.8, and predicted to be the primary mineral phase at the final pH (12.4) of the Hg–Al-cpt system (Figure 4A), in agreement with experimental observations.

In the Hg–Fe-cpt system, thermodynamic analysis predicts the formation of a Ca–Fe-sulfate-hydrate phase ($(\text{Ca}_4\text{Fe}_2\text{SO}_4)_-(\text{OH})_{12} \cdot 6\text{H}_2\text{O}$) at the measured pH of the final solution (12.6), which is not in agreement with the observed formation of gypsum as the primary mineral phase and the inferred precipitation of ferrihydrite (Figure 4B). The observed solids are the metastable assemblage predicted at slightly lower pH (<11.8) and suggest that the system may not have reached equilibrium with respect to solid phases. Prior work noted the slow kinetics of Fe-etagringite formation (180 days to reach equilibrium) relative to Al-etagringite, and the initial formation of ferrihydrite and gypsum in Al-free systems.^{10,11} There is also uncertainty in both the stoichiometries and solubilities of hydrated Ca–Fe hydroxysulfate phases that may form at high pH,^{39,40} which would change the positions of the stability fields shown in Figure 4B. In the Fe-cpt without Hg, a Ca–Fe-sulfate-hydrate phase (of different stoichiometry than the phase used in the thermodynamic database) and calcite (as a minor phase) were identified as reaction products by XRD. The presence of calcite indicates that, despite efforts to exclude CO_2 during sample preparation, some CO_2 contamination did occur. However, calcite was not identified in the other experiments and there is no evidence for CO_2 contamination. Since all solids were prepared under the same experimental conditions, carbonate activities in the system should be much lower than sulfate activities, and the formation of other mineral phase containing CO_2 is not expected.¹⁰

Based on chemical analyses of precipitated solids and extraction results, most Hg was associated with recalcitrant mineral phases in the coprecipitate systems, with ~20–25% of total Hg easily exchanged. Based on thermodynamic analysis of Hg speciation, $\text{HgCl}_2(\text{aq})$ is the dominant equilibrium aqueous species predicted at the initial Cl^- concentration and pH of both systems, but $\text{Hg}(\text{OH})_2^0$ is the dominant equilibrium species predicted at the final pH (Figure 4). Therefore, if equilibrium among aqueous Hg species is reached, Hg–Cl coordination would not be expected. Results from Hg EXAFS analysis showed coordination of Hg by Cl ligands in Hg–Al-cpt solids, and no coordination by O or S (as sulfate) ligands. These observations imply that molecular Hg–Cl complexation in the initial aqueous state is preserved in the final solids, and that Hg species do not equilibrate at the final solution pH in the Fe-free system. Evidence from Hg EXAFS, spatial analysis, and thermodynamic considerations suggest physical encapsulation of Hg as a salt precipitate with ettringite as the primary immobilization mechanism. This Hg sequestration mechanism, after the addition of cement and other alkali amendments, has been proposed in the literature,^{14,16,44} although the proposed form of immobilized Hg was HgO(s) in most prior studies.

In the Hg–Fe-cpt system, only O ligands were identified in the first shell in the Hg EXAFS analysis, but no coordination with Cl^- or SO_4^{2-} ligands. Because $\text{Hg}(\text{OH})_2^0$ is the dominant

equilibrium species predicted at the final pH, Hg is inferred to re-equilibrate from the initial conditions where HgCl_2 is the dominant aqueous species, to $\text{Hg}(\text{OH})_2^0$ as the dominant species. Mercury XAS results indicated coprecipitation of Hg and ferrihydrite, with most Hg strongly bonded to ferrihydrite based on the extraction results showing that only ~20% of total Hg was removed by ion exchange. In the sorption systems with 25 times less total Hg, less than 1% of sorbed Hg is exchangeable (up to 30 d reaction time). These results are in agreement with prior studies of Hg sorption on Fe(III) oxides that interpreted most sorbed Hg as inner-sphere complexes with a smaller fraction of outer-sphere complexes.^{25,26,42,43} Although Hg bonds as an inner-sphere complex to Fe(III) oxide surfaces, ferrihydrite tends to retain water within an open network structure of Fe octahedra that allows for diffusion of aqueous species.⁴⁵ Results of the Hg EXAFS analysis suggest that Hg coprecipitated with ferrihydrite in the Hg–Fe-cpt solids were sufficiently hydrated to allow for re-equilibration of the sorbed Hg species with the solution as pH increased.

4.3. Implications. Mercury immobilization by precipitation and/or complexation in solid phases is a remediation strategy that may aid in limiting Hg trophic transfer. Results of this study indicate that remediation approaches should emphasize physical encapsulation of Hg, perhaps as a nanoparticulate phase, within reaction products rather than formation of mineral solid solutions or surface adsorption. Complexation of Hg by chloride influences Hg behavior during formation of cement product phases. Therefore, differences between freshwater and marine/estuarine settings should be considered in remediation design. In addition, physical differences in porosity and extent of hydration of reaction products can influence rates of Hg uptake and its final distribution in product phases. This study highlights an important role for Fe in both Hg removal from solution and remediation scenarios. The presence of Fe in cement treatments of soils or sediment may affect the rate of ettringite formation and its stability through formation of an immiscible Al–Fe solid solution,¹¹ although characterization and thermodynamic data for such phases are incomplete. In natural systems, strong complexation of Hg with thiol and sulfide functional groups of dissolved and sediment organic matter are likely to outcompete Fe(III) oxide surfaces for binding Hg.^{46,47} However, in dynamic environments such as groundwater–surface water transition zones, dissolved Fe^{2+} may oxidize and rapidly precipitate as ferrihydrite, which can scavenge dissolved Hg as a sorbed complex as shown here, particularly if organic carbon is low. Therefore, relative concentrations of organic matter and Fe, and the dynamic biogeochemical processes associated with these constituents that influence Hg speciation and transport, should be considered in site-specific risk assessment and remediation design. Examination of the model systems of this study lends insight into the chemical behavior of Hg and the physical processes that occur during reaction with cementitious materials. Studies of specific applications and treatment systems are needed to verify microscale mechanisms over a broad range of conditions.

ASSOCIATED CONTENT

S Supporting Information

Description of the analyses of aqueous solutions, mercury (low concentration) sorption and chemical extractions experiments, S and Hg X-ray absorption spectroscopy (XAS) methods description, and XAS analysis of Hg reference compounds; bulk

XRD analysis of coprecipitate products (Figure S1); elemental analysis of coprecipitate phases and supernatant solution (Tables S1 and S2, respectively); Hg (low concentration) sorption analysis (Table S3); thermodynamic data for equilibrium calculations (Table S4); XAS fit results of Hg reference compounds (Figures S2 and S3 and Table S5). This material is available free of charge via the Internet at <http://pubs.acs.org>.

AUTHOR INFORMATION

Corresponding Author

*Phone: +34 91 745 2500; fax: +34 91 564 08 00; e-mail: susana.serrano@ica.csic.es.

Present Address

^{II}Institute for Agricultural Sciences, Consejo Superior de Investigaciones Científicas (CSIC), Serrano 115-dup, 28006-Madrid, Spain.

Notes

The authors declare no competing financial interest.

ACKNOWLEDGMENTS

This research was supported by funding from the NIH-NIEHS Superfund Research Program (R01 ES016201). Portions of this research were carried out at the Stanford Synchrotron Radiation Lightsource, a national user facility operated by Stanford University on behalf of the U.S. Department of Energy, Office of Basic Energy Sciences. Thanks to Ken Dominik (University of Arizona Electron Microprobe Laboratory) for electron microprobe data collection. We thank S. S. Papadopoulos & Associates and Anchor QEA, LLC for additional support.

REFERENCES

- Ward, D. M.; Nislow, K. H.; Folt, C. L., Bioaccumulation syndrome: Identifying factors that make some stream food webs prone to elevated mercury bioaccumulation. In *Year in Ecology and Conservation Biology 2010*; Ostfeld, R. S.; Schlesinger, W. H., Eds.; 2010; Vol. 1195, pp 62–83.
- Mergler, D.; Anderson, H. A.; Chan, L. H. M.; Mahaffey, K. R.; Murray, M.; Sakamoto, M.; Stern, A. H. Methylmercury exposure and health effects in humans: A worldwide concern. *Ambio* 2007, 36, 3–11.
- Ulrich, P. D.; Sedlak, D. L. Impact of iron amendment on net methylmercury export from tidal wetland microcosms. *Environ. Sci. Technol.* 2010, 44 (19), 7659–7665.
- O'Day, P. A.; Vlassopoulos, D. Mineral-based amendments for remediation. *Elements* 2010, 6, 375–381.
- Koski, R. A.; Munk, L.; Foster, A. L.; Shanks, W. C.; Stillings, L. L. Sulfide oxidation and distribution of metals near abandoned copper mines in coastal environments, Prince William Sound, Alaska, USA. *Appl. Geochem.* 2008, 23 (2), 227–254.
- Warren, C. J.; Reardon, E. J. The solubility of ettringite at 25 °C. *Cem. Concr. Res.* 1994, 24 (8), 1515–1524.
- Albino, V.; Cioffi, R.; Marrocchini, M.; Santoro, L. Potential application of ettringite generating systems for hazardous waste stabilization. *J. Hazard. Mater.* 1996, 51 (1–3), 241–252.
- Perkins, R. B.; Palmer, C. D. Solubility of ettringite ($\text{Ca}_6[\text{Al}(\text{OH})_6]_2(\text{SO}_4)_3 \cdot 26\text{H}_2\text{O}$) at 5–75°C. *Geochim. Cosmochim. Acta* 1999, 63 (13–14), 1969–1980.
- Chrysocou, M.; Dermatas, D. Evaluation of ettringite and hydrocalumite formation for heavy metal immobilization: Literature review and experimental study. *J. Hazard. Mater.* 2006, 136 (1), 20–33.
- Moschner, G.; Lothenbach, B.; Rose, J.; Ulrich, A.; Figi, R.; Kretzschmar, R. Solubility of Fe-ettringite ($\text{Ca}_6[\text{Fe}(\text{OH})_6]_2(\text{SO}_4)_3 \cdot 26\text{H}_2\text{O}$). *Geochim. Cosmochim. Acta* 2008, 72 (1), 1–18.
- Moschner, G.; Lothenbach, B.; Winnefeld, F.; Ulrich, A.; Figi, R.; Kretzschmar, R. Solid solution between Al-ettringite and Fe-ettringite ($\text{Ca}_6[\text{Al}_{1-x}\text{Fe}_x(\text{OH})_6]_2(\text{SO}_4)_3 \cdot 26\text{H}_2\text{O}$). *Cem. Concr. Res.* 2009, 39 (6), 482–489.
- Guha, B.; Hills, C. D.; Carey, P.; MacLeod, C. L. Leaching of mercury from carbonated and non-carbonated cement-solidified dredged sediments. *Soil Sed. Contam.* 2006, 15, 621–635.
- Careghini, A.; Dastoli, S.; Ferrari, G.; Saponaro, S.; Bonomo, L. Sequential solidification/stabilization and thermal process under vacuum for the treatment of mercury in sediments. *J. soils sed.* 2010, 10 (8), 1646–1656.
- Poon, C. S.; Peters, C. J.; Perry, R.; Barnes, P.; Barker, A. P. Mechanisms of metal stabilization by cement based fixation processes. *Sci. Total Environ.* 1985, 41 (1), 55–71.
- Cocke, D. L. The binding chemistry and leaching mechanisms of hazardous substances in cementitious solidification stabilization systems. *J. Hazard. Mater.* 1990, 24 (2–3), 231–253.
- McWhinney, H. G.; Cocke, D. L.; Balke, K.; Ortego, J. D. An investigation of mercury solidification and stabilization in Portland-cement using X-ray photoelectron-spectroscopy and energy dispersive spectroscopy. *Cem. Concr. Res.* 1990, 20 (1), 79–91.
- Roy, A.; Eaton, H. C.; Cartledge, F. K.; Tittlebaum, M. E. Solidification stabilization of a heavy-metal sludge by a portland-cement fly-ash binding mixture. *Hazard. Waste Hazard. Mater.* 1991, 8 (1), 33–41.
- Roy, A.; Eaton, H. C.; Cartledge, F. K.; Tittlebaum, M. E. Solidification stabilization of hazardous-waste—Evidence of physical encapsulation. *Environ. Sci. Technol.* 1992, 26 (7), 1349–1353.
- Zhuang, J. M.; Lo, T.; Walsh, T.; Lam, T. Stabilization of high mercury contaminated brine purification sludge. *J. Hazard. Mater.* 2004, 113 (1–3), 157–164.
- Chen, J.; Chen, H.; Jin, X.; Chen, H. Determination of ultra-trace amount methyl-, phenyl- and inorganic mercury in environmental and biological samples by liquid chromatography with inductively coupled plasma mass spectrometry after cloud point extraction preconcentration. *Talanta* 2009, 77 (4), 1381–1387.
- Johansson, G. On the structures of the hydrolysis complexes of mercury (II) in solution. *Acta Chem. Scand.* 1971, 25, 2799–2806.
- House, D. A.; Robinson, W. T.; McKee, V. Chloromercury(II) anions. *Coordin. Chem. Rev.* 1994, 135–136, 533–586.
- Barrow, N. J.; Cox, V. C. The effects of pH and chloride concentration on mercury sorption. I. By goethite. *J. Soil Sci.* 1992, 43 (2), 295–304.
- Gunneriusson, L.; Sjoberg, S. Surface complexation in the H^+ -goethite ($[\alpha\text{-FeOOH}]$ -Hg (II)-chloride system. *J. Colloid Interface Sci.* 1993, 156 (1), 121–128.
- Kim, C. S.; Rytuba, J.; Brown, G. E. EXAFS study of mercury(II) sorption to Fe- and Al-(hydr)oxides. II. Effects of chloride and sulfate. *J. Colloid Interface Sci.* 2004, 270 (1), 9–20.
- Kim, C. S.; Rytuba, J. J.; Brown, G. E. EXAFS study of mercury(II) sorption to Fe- and Al-(hydr)oxides I. Effects of pH. *J. Colloid Interface Sci.* 2004, 271 (1), 1–15.
- Odler, I.; Abdulmaula, S. Possibilities of quantitative-determination of the AFt-(ettringite) and AFm-(monosulfate) phases in hydrated cement pastes. *Cem. Concr. Res.* 1984, 14 (1), 133–141.
- De Stefano, C.; Foti, C.; Sammartano, S.; Gianguzza, A.; Rigano, C. Equilibrium studies in natural fluids. Use of simulated seawater and other media as background salt. *Anal. Chim. Rome* 1994, 84, 159–175.
- Gómez Ariza, J. L.; Giráldez, I.; Sánchez-Rodas, D.; Morales, E. Selectivity assessment of a sequential extraction procedure for metal mobility characterization using model phases. *Talanta* 2000, 52 (3), 545–554.
- Schwertmann, U.; Cornell, R. M. *Iron Oxides in the Laboratory: Preparation and Characterization*; Wiley-VCH: Weinheim, Germany, 1991; p 137.
- Webb, S. M. Sixpack: a graphical user interface for XAS analysis using IFEFFIT. *Phys. Scr.* 2005, T115, 1011–1014.

- (32) George, G. N.; Pickering, I. J. EXAFSPAK: A Suite of Computer Programs for Analysis of X-ray Absorption Spectra; Stanford Synchrotron Radiation Laboratory: Stanford, CA, 2000.
- (33) Delany, J. M.; Lundeen, S. R., *The LLNL Thermochemical Database, Lawrence Livermore National Laboratory Report*. Lawrence Livermore National Laboratory Report: Livermore, CA, 1994.
- (34) Lothenbach, B.; Winnefeld, F. Thermodynamic modelling of the hydration of Portland cement. *Cem. Concr. Res.* **2006**, *36* (2), 209–226.
- (35) Powell, K. J.; Brown, P. L.; Byrne, R. H.; Gajda, T.; Hefta, G.; Sjoberg, S.; Wanner, H. Chemical speciation of environmentally significant heavy metals with inorganic ligands. Part 1: The Hg^{2+} , Cl^- , OH^- , CO_3^{2-} , SO_4^{2-} , and PO_4^{3-} aqueous systems. *Pure Appl. Chem.* **2005**, *77*, 739–800.
- (36) Drits, V. A.; Sakharov, B. A.; Salyn, A. L.; Manceau, A. Structural model for ferrihydrite. *Clay Miner.* **1993**, *28* (2), 185–207.
- (37) Barnum, D. W. Hydrolysis of cations. Formation constants and standard free energies of formation of hydroxy complexes. *Inorg. Chem.* **1983**, *22* (16), 2297–2305.
- (38) Wen, H.; Miller, S. E.; House, D. A.; McKee, V.; Robinson, W. T. The crystal-structures of some chloromercury(II) anions with Co(III) complexes or protonated polyamines as cations. *Inorg. Chim. Acta* **1992**, *193* (1), 77–85.
- (39) Putzas, D.; Rotter, H. W.; Thiele, G.; Brodersen, K.; Pezzei, G. Die Kristallstruktur von $2\text{CaCl}_2 \cdot 11\text{HgCl}_2 \cdot 16\text{H}_2\text{O}$, eines kubischen, quecksilberreichen Chloromercurats mit ikosaedrischen $\text{Hg}_6\text{Cl}_{13}^-$ und $\text{Hg}_5\text{Cl}_{13}^-$ -Baugruppen. *Z. Anorg. Allg. Chem.* **1991**, *595* (1), 193–202.
- (40) Brodersen, K.; Pezzei, G.; Thiele, G. Crystal-structure of the magnesium octachlorotrimercurate(II)-hexahydrate $\text{MgHg}_3\text{Cl}_8 \cdot 6\text{H}_2\text{O}$. *Z. Anorg. Allg. Chem.* **1983**, *499* (4), 169–174.
- (41) House, D. A.; McKee, V.; Robinson, W. T. The crystal structures of chloro mercury(II) salts found for some CrN_6^{3+} cations and their Cr—N bond-ruptured hydrolysis products. *Inorg. Chim. Acta* **1989**, *157* (1), 15–27.
- (42) Slowey, A. J.; Brown, G. E. Transformations of mercury, iron, and sulfur during the reductive dissolution of iron oxyhydroxide by sulfide. *Geochim. Cosmochim. Acta* **2007**, *71* (4), 877–894.
- (43) Bargar, J. R.; Persson, P.; Brown, G. E. XAFS studies of Pb(II)-chloro and Hg(II)-chloro ternary complexes on goethite. *J. Phys. IV* **1997**, *7* (C2), 825–826.
- (44) Qian, G.; Delai Sun, D.; Hwa Tay, J. Characterization of mercury- and zinc-doped alkali-activated slag matrix: Part I. Mercury. *Cem. Concr. Res.* **2003**, *33* (8), 1251–1256.
- (45) Axe, L.; Trivedi, P. Intraparticle surface diffusion of metal contaminants and their attenuation in microporous amorphous Al, Fe, and Mn Oxides. *J. Colloid Interface Sci.* **2002**, *247* (2), 259–265.
- (46) Drott, A.; Lambertsson, L.; Bjorn, E.; Skyllberg, U. Importance of dissolved neutral mercury sulfides for methyl mercury production in contaminated sediments. *Environ. Sci. Technol.* **2007**, *41* (7), 2270–2276.
- (47) Feyte, S.; Tessier, A.; Gobeil, C.; Cossa, D. In situ adsorption of mercury, methylmercury and other elements by iron oxyhydroxides and organic matter in lake sediments. *Appl. Geochem.* **2010**, *25* (7), 984–995.